Journal of Inorganic Biochemistry 203 (2020) 110952

Contents lists available at ScienceDirect

Journal of Inorganic Biochemistry

journal homepage: www.elsevier.com/locate/jinorgbio

Influence of synthesis methods on the internalization of fluorescent gold nanoparticles into glioblastoma stem-like cells

Beatriz Giesen[a], Ann-Christin Nickel[b], Alba Garzón Manjón[c], Andrés Vargas Toscano[b], Christina Scheu[c], Ulf Dietrich Kahlert[b,d,*], Christoph Janiak[a,*]

[a] Institut für Anorganische Chemie und Strukturchemie, Heinrich-Heine-Universität Düsseldorf, 40204 Düsseldorf, Germany
[b] Klinik für Neurochirurgie, Universitätsklinikum Düsseldorf, 40225 Düsseldorf, Germany
[c] Max-Planck-Institut für Eisenforschung GmbH, Max-Planck-Straße 1, 40237 Düsseldorf, Germany
[d] Deutsches Konsortium für Translationale Krebsforschung (DKTK), Essen/Düsseldorf, Germany

ARTICLE INFO

Keywords:
Fluorescent gold nanoparticles
Precision medicine
Rapid synthesis
Glioblastoma stem cells
Internalization

ABSTRACT

Glioblastoma (GBM) is an aggressive disease with currently no satisfying treatment option available. GBM cells with stem cell properties are thought to be responsible for the initiation and propagation of the disease, as well as main contributors to the emergence of therapy resistance. In this work, we developed a novel method to synthesize fluorescent gold nanoparticles as potential drug and gene delivery systems for GBM therapy, able to penetrate three-dimensional stem cell selected patient-derived GBM neurosphere systems *in vitro*. By using polyethylene imine (PEI) as a stabilizer and reducing agent, as well as fluorescein isothiocyanate (FITC) as a fluorescent marker, our fully *in-house* developed fluorescent gold nanoparticles (AuPEI-FITC NPs) with core sizes between 3 and 6 nm were obtained *via* a fast microwave-assisted reaction. Cytotoxicity, adsorption and internalization of AuPEI-FITC NPs into the cell lines JHH520, 407 and GBM1 were investigated using the cellular growth assay and fluorescence-activated cell sorting (FACS) analysis. AuPEI-FITC NPs showed no apparent cytotoxicity and an uptake in cells of up to ~80%. A differentiation between surface-bound and internalized AuPEI-FITC NPs was possible by quenching extracellular signals. This resulted in a maximal internalization degree of 61%, which depends highly on the synthesis method of the nanoparticles and the cell type tested. The best internalization was found for AuPEI-FITC1 which was prepared in a one pot reaction from $KAuCl_4$, PEI and FITC. Thus, appropriately synthesized AuPEI-FITC NPs show great potential as vehicles to transport DNA or drugs in GBM cells.

1. Introduction

Glioblastoma (GBM), the most common type of brain-born neoplasm, is a lethal and ultra-aggressive type of cancer with a remaining life expectancy of under two years [1]. Current therapy consists of surgical resection, administration of temozolomide and radiotherapy but fails to give a positive outcome due to the invasive and heterogeneous nature of the tumor [2]. A population of cells with stem cell properties (= brain cancer stem-like cells, BCSCs) are thought to be the reason for GBM's high cellular invasion capacity and formation of tumor foci [3]. Delivery of therapeutics to the anticipated BCSCs target site is significantly hindered by the blood-brain barrier (BBB), a major obstacle in GBM treatment [4]. Thus, novel anti-BCSC treatments with clinical applicability are of highest clinical and economical interest.

Recent studies have placed nanomaterials in the focus as the future technology for the delivery of drugs, molecules or genes to treat GBM, specifically by targeting BCSCs [5,6]. Gold nanoparticles (Au-NPs) in particular have been widely used for medicinal purposes due to their biocompatibility and unique optical properties. Due to the high permeability and enhanced permeation and retention (EPR) in solid tumors, Au-NPs can pass the BBB, accumulate in the damaged tissue and deliver inhibiting or target specific cell surface molecules like proteins or antibodies, which limit tumor cell proliferation and boost the anticancer effect of standard drugs [6–9]. In combination with radiotherapy, Au-NPs increase the DNA damage to GBM cells inflicted by ionization radiation [10]. This radiosensitization enhances the effectivity of irradiation therapy and also improves the uptake of medications in GBM cells [11,12]. Besides their therapeutic benefits, Au-NPs are also widely used for imaging and sensing applications, showing a longer blood circulation time than common contrast agents [13]. They

* Corresponding author's.
E-mail addresses: Ulf.Kahlert@med.uni-duesseldorf.de (U.D. Kahlert), janiak@uni-duesseldorf.de (C. Janiak).

https://doi.org/10.1016/j.jinorgbio.2019.110952
Received 17 September 2019; Received in revised form 14 November 2019; Accepted 22 November 2019
Available online 23 November 2019
0162-0134/

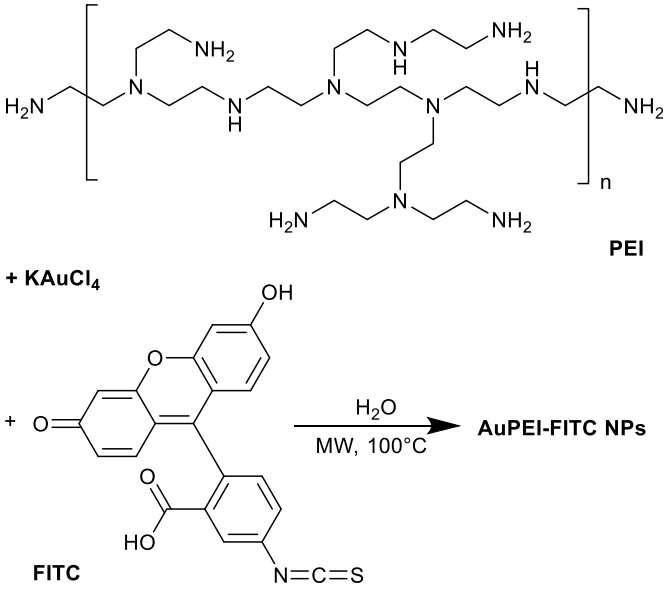

Scheme 1. Representation of the synthesis protocol for optimized AuPEI-FITC NPs for the internalization into glioblastoma GBM cells.

have allowed the accurate display of tumors for its surgical removal due to their surface enhanced resonance Raman scattering (SERRS) signals in combination with magnetic resonance imaging (MRI), as well as being introduced as precise probes for computer tomography (CT) and photoacoustic visualization of tumors [14–16]. In summary, Au-NPs are promising theranostic systems combining therapeutic anticancer effects with diagnostic features for tracking the biodistribution of GBM tumors *in vivo*.

The aqueous synthesis of Au-NPs is straight-forward, cost effective and non-toxic. Moreover, the highly stable colloids formed are modifiable in size and shape through variation of their synthesis parameters. Their surface can be functionalized with various capping ligands and shells to facilitate the loading of therapeutic agents according to specific cell or drug needs [17]. In gene therapy, polyethylene imine (PEI) (Scheme 1) constitutes a suitable capping ligand for Au-NPs because of its high cationic charge density and ability to condensate nucleic acids to the nanoparticle (NP) surface [18]. In the chemical reaction with gold, PEI acts as a three-in-one reagent: it can reduce gold(III) salts to metallic gold, it protects the formed Au-NPs from agglomeration and it can bind DNA through electrostatic interactions [19].

In nanodelivery applications, fluorescein isothiocyanate (FITC) (Scheme 1), a near-infrared organic dye, can serve as a powerful tracking device to locate NPs inside the cells after incubation due to its high extinction coefficient and great quantum yield. Due to the strong affinity of gold for sulfur, FITC can be effectively coupled to Au-NPs though electronically stable covalent bonds with its isothiocyanate group [20]. This Au-FITC combination holds a stronger fluorescent imaging effect of tumor regions compared to FITC alone, which would rapidly be metabolized and removed by cells [10]. When obtained from commercial sources, little information is given about the capping ligand of fluorescent Au-NPs, the amount of fluorophore used and, in some cases, the overall hydrodynamic size of the gold-ligand-FITC system, which is crucial for cell uptake. If the nanodelivery technology is going to become standard, there needs to be easy, reliable and fast methods to produce fluorescent nanocarriers without the need to resort to expensive outsourcing or intricate synthesis routes.

In this work, we describe a Au-NP assembly functionalized with PEI and FITC (AuPEI-FITC) able to penetrate GBM cells. AuPEI-FITC NPs were synthesized in a straight-forward manner from cheap and accessible starting materials (Scheme 1). We describe the importance of the synthesis parameters on the final size, morphology and ligand composition of the nanomaterials even when using the same components. Our GBM functional assessments are performed with three-dimensional neurospheres, selected for high percentage of stemness due to neural stem cell growth conditions [21]. The *in vitro* AuPEI-FITC NPs transfection and level of internalization in three BCSC lines are hereby tested for a potential application as a gene or drug carrier in the treatment of GBM.

2. Results and discussion

2.1. Synthesis of gold nanoparticles

Regardless of the various works stating to have found the ideal nanoparticle size and shape for a successful internalization into cells [22–24], the actual impact of these parameters still remains highly dependent on the cell type. In this study, we opted for the synthesis of small gold nanospheres up to 10 nm diameter. By starting with a small core size, multiple functionalization steps on the nanoparticle surface are possible through a layer-by-layer construct, which allows flexibility to customize and increase the size of the carrier if needed. Furthermore, round-shaped Au-NPs were selected due to their curvature, which makes them more likely to be internalized into cells compared to asymmetrical shaped NPs [25].

The synthesis of gold nanoparticles smaller than 20 nm has been documented by adding a tetrachloroaurate precursor into an aqueous PEI solution under diverse reaction conditions [19,26,27]. Size control is not always easy since a stoichiometric variation of reaction precursors also changes the size distribution and polydispersity of the solution. In order to find the necessary gold to PEI ratio for an optimal stabilization of our delivery system, the amount of $KAuCl_4$ precursor added to a solution of branched PEI was continuously increased as both components were reacted under microwave irradiation (see Supp. info. for synthesis details). Variation of the n_{KAuCl4}/n_{PEI} molar ratio between 1 and 10 (samples AuPEI1–10 accordingly) resulted in different sizes and polydispersity values, as seen from dynamic light scattering (DLS) results (Fig. 1). In our experiments, hydrodynamic diameters corresponding to the gold core and the PEI capping ligand remained between 24 and 67 nm. In some cases, various species of different sizes were detected even after post-synthesis purification. This phenomenon can be attributed to the formation of higher bridged PEI networks containing several Au cores [7].

However, there seems be an optimal ratio of PEI to Au, resulting in small AuPEI NPs with low polydispersity, as in the case of AuPEI5 and

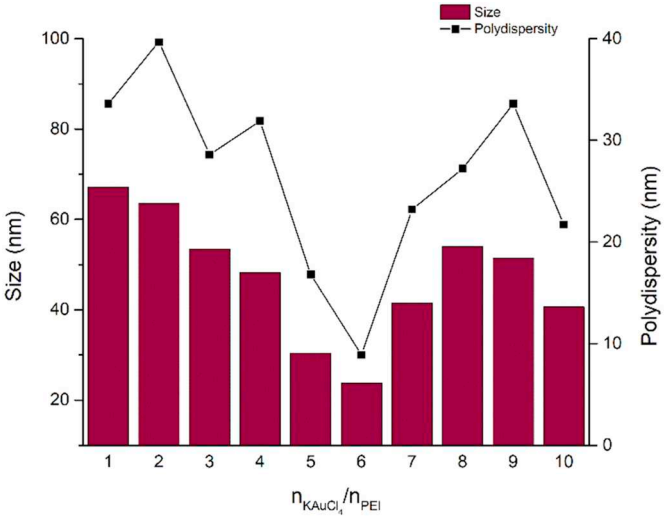

Fig. 1. Size and polydispersity of PEI-capped gold nanoparticles (Au-PEI NPs) with n_{KAuCl4}/n_{PEI} = 1–10.

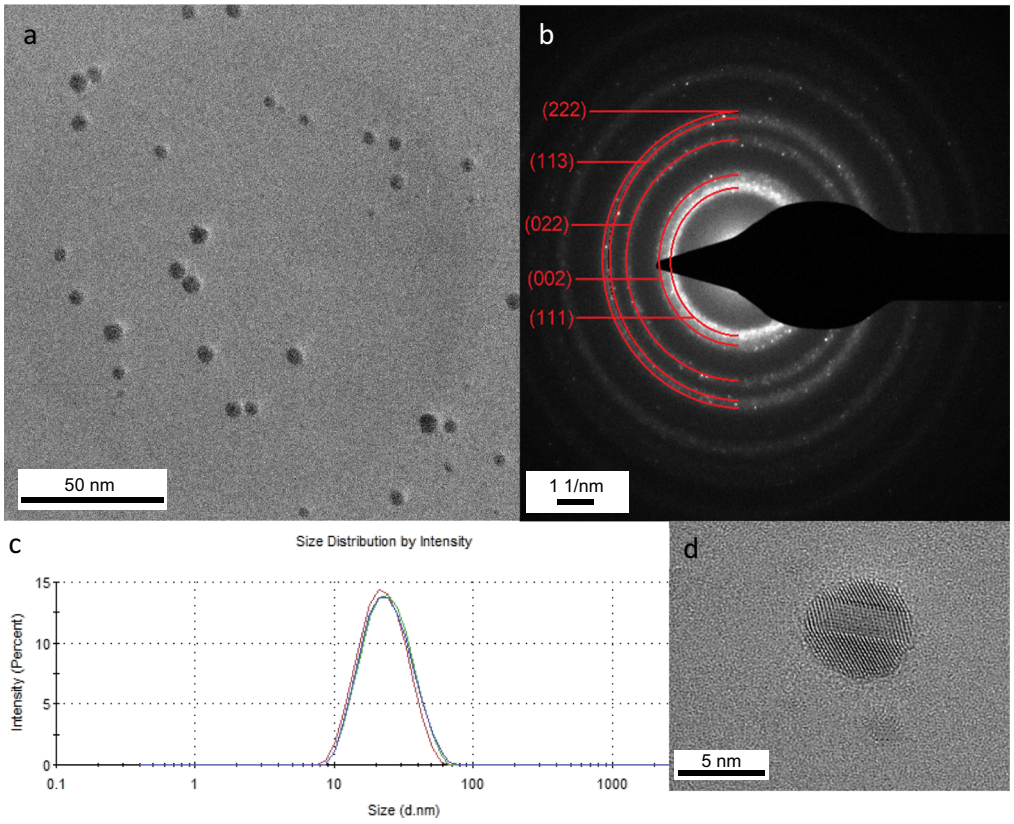

Fig. 2. Characterization of AuPEI6 NPs. a, TEM image of several NPs, b: selected area diffraction showing *hkl* values for *fcc* gold, c: DLS curve showing the size distribution by intensity of three measurements, d: HR-TEM image of an individual NP.

AuPEI6 with $n_{KAuCl4}/n_{PEI} = 5$ or 6, respectively. With a hydrodynamic diameter of 24 nm and a narrow size distribution, AuPEI6 presented the most homogeneous sample. The small size of AuPEI6 NPs was further confirmed *via* high-resolution transmission electron microscopy (HR-TEM) measurements, which revealed a gold core of about 4 ± 1 nm (Fig. 2). The sample also displayed high crystallinity and the expected face-centered cubic (*fcc*) phase.

In the reaction of $KAuCl_4$ and PEI, Au-NPs are formed due to a redox reaction between the amine groups of PEI and the tetrachloridoaurate (III) anion $AuCl_4^-$. While the Au^{III} salt is reduced to Au^0, oxidation at the alpha carbon to the amine groups of the PEI polymer chain results in the conversion of the amine into an amide [27]. This assumption was confirmed by infrared (IR) spectroscopy (Fig. S1 in SI).

Given that PEI itself has also been used as a vehicle for DNA transfection [28], it is crucial to eliminate the free unbound PEI from the gold solution in order to test the true ability of AuPEI NPs as a DNA or drug carrier. For this purpose, a thorough dialysis process was performed against water for 24 h (see Supp. info. for details, Fig. S2). When dialyzing the sample AuPEI6 for a longer time, a significant color change from dark red to purple was observed, signaling a size increase of AuPEI NPs due to a possible agglomeration. DLS results showed an increase in hydrodynamic diameter from 24 nm after 24 h to 68 nm after 48 h and ultimately 77 nm after 72 h. On the other hand, when the sample was left to dialyze for only 6 or 12 h, agglomerates of "free" PEI as large as 91 nm were still found in the sample. Thus, determination of the correct dialysis time is relevant to remove both polymer accumulations in the solution or unstable NP agglomerates which lack stabilization.

TEM images and ultraviolet–visible (UV–VIS) spectra of AuPEI6 before and after 24 h of dialysis (Fig. 3) show the importance of purification for obtaining a more homogeneous Au-NP solution. After dialysis, it was possible to remove larger agglomerates from the initial sample (Fig. 3a, b) and a narrowing of the plasmonic band at 525 nm was observed (Fig. 3c). The resulting AuPEI NPs had a size of 4 ± 1 nm. NPs of this size have successfully loaded drug molecules onto their surface and would be able to exit the body by renal excretion after drug release [29].

Subsequently, the FITC fluorophore was introduced into the AuPEI system as a NP tracking tool in the cells. Several synthesis and purification approaches were tested in order to find a suitable NP species by varying the FITC concentration, the reaction media and ligand incorporation method (Table S1). As a preliminary verification, the cell viability of human embryonic kidney cells (HEK) was monitored after 1 and 3 h of incubation with AuPEI-FITC1–10 NPs at a gold concentration between 0 and 50 mg/L (Fig. S4). Using low toxicity and a good concentration dependence as relevant criteria, samples AuPEI-FITC 1–4 were chosen for further testing in GBM cells. In these four different synthesis approaches, the reaction starting components (gold precursor, PEI and FITC) were introduced at the same ratios but in different order (Fig. 4). Reduction of the gold precursor was always achieved in a hydrothermal microwave reaction, using only PEI as the reducing agent. UV–VIS results of the four samples revealed the characteristic plasmonic peak of Au-NPs at 500 nm (Fig. S5). Solution colors ranged from light orange-red to brownish-red (Fig. S6). Size and size distribution results determined by DLS and TEM for all four synthesis routes are shown in Table S2 and Fig. S7. The morphology of the samples AuPEI-FITC1–4 is displayed in Fig. 5.

Our novel preparation of AuPEI-FITC1 through a so-called "one-pot" synthesis, resulted in the formation of small nanospheres with an average gold core of 3 ± 1 nm. Preformed AuPEI NPs were prepared with the AuPEI6 protocol (see above). When these preformed AuPEI NPs were reacted with the same amount of FITC used for AuPEI-FITC1, similar sized NPs were obtained (AuPEI-FITC2). In the last two experiments, FITC was first linked to the polymer as a PEI-FITC conjugate

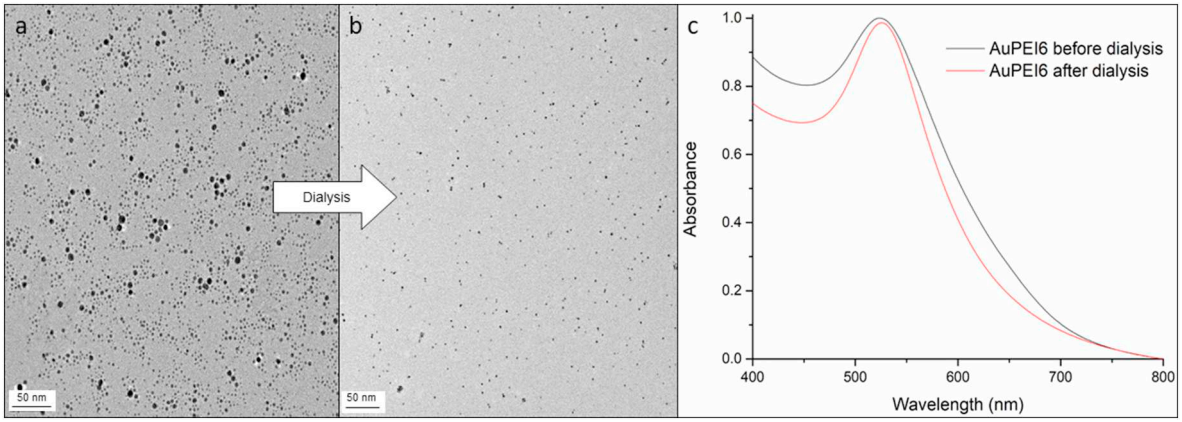

Fig. 3. Effect of purification *via* dialysis of AuPEI6. TEM micrographs of Au-NPs a: before and b: after dialysis. c: Absorbance data. The histograms and DLS measurements for the AuPEI6 NPs before and after dialysis are shown in Fig. S3, Supp. info.

and then either mixed with the preformed AuPEI NPs (for AuPEI-FITC4) or combined with an aqueous solution of $KAuCl_4$ followed by the reduction of the gold(III) precursor (for AuPEI-FITC3). For all cases, a microwave reaction at 100 °C using FITC is possible since the thiocyanate compound shows a decomposition temperature of 260 °C, according to thermogravimetric analysis results (Fig. S8).

In the case of AuPEI-FITC3, previously linking FITC to PEI resulted in the formation of a mixture of two species of NPs with slightly different sizes (Fig. 5c). Even though the PEI-FITC conjugate was purified to eliminate unbound components, there is the possibility that PEI remained either unlabeled or was separated from FITC during the thermal treatment. The parallel existence of both PEI and PEI-FITC in the solution is most likely responsible for two separate nucleation and growth processes of the Au colloids, which could result in different sized NP products. Similarly, a direct stabilization of Au-NPs by FITC instead of PEI cannot be ruled out due to the strong attraction of its thiocyanate group towards gold.

The presence of the fluorescent FITC marker on AuPEI NPs was confirmed using scanning transmission electron microscopy (STEM). Energy-dispersive X-ray spectroscopy (EDX) measurements in STEM mode were able to identify gold atoms corresponding to Au-NPs, as well as sulfur atoms from the FITC ligand in the same area. Both gold and sulfur signals are displayed in color-coded elemental maps in Figs. 6 and S9. Hence, the attachment of FITC to the surface of all AuPEI-FITC NP samples was verified. Additionally, this attachment was verified to be pH resistant between pH 6 and 8, as proven for AuPEI-FITC1 NPs in different phosphate buffers (see Fig. S10).

Due to the high extinction coefficient of Au-NPs and the overlap of their surface plasmon resonance peak with the emission maximum of FITC at 517 nm (Fig. S5), a fluorescence resonance energy transfer (FRET) from FITC to the Au-NPs can be expected [30]. As FITC interacts with the Au-NPs, its fluorescence is severely quenched, which allows further confirmation of a successful functionalization of FITC onto the gold surface. Even though the same amount of FITC was used for all AuPEI-FITC synthesis reactions, fluorescence measurements displayed various degrees of quenching, most likely due to different interactions between FITC and gold atoms in each sample (Fig. S11a).

As expected, all AuPEI-FITC solutions exhibited a lower fluorescence than the FITC control, thereby supporting the attachment of FITC onto the NP surface. AuPEI-FITC1 and AuPEI-FITC3 showed similar fluorescence intensities, contrary to the other two samples. AuPEI-FITC2 exhibited the highest fluorescence intensity (still about 50% less than the FITC control) and AuPEI-FITC4 the lowest (75% less than FITC) of all four NP types. In this case, a lower fluorescence can be the result of a stronger quenching effect and/or a lower amount of FITC being attached to the gold surface. In order to rule out the fluorescence detection from “free” FITC in the solution, AuPEI-FITC samples were centrifuged and the spectra from their supernatants were also recorded

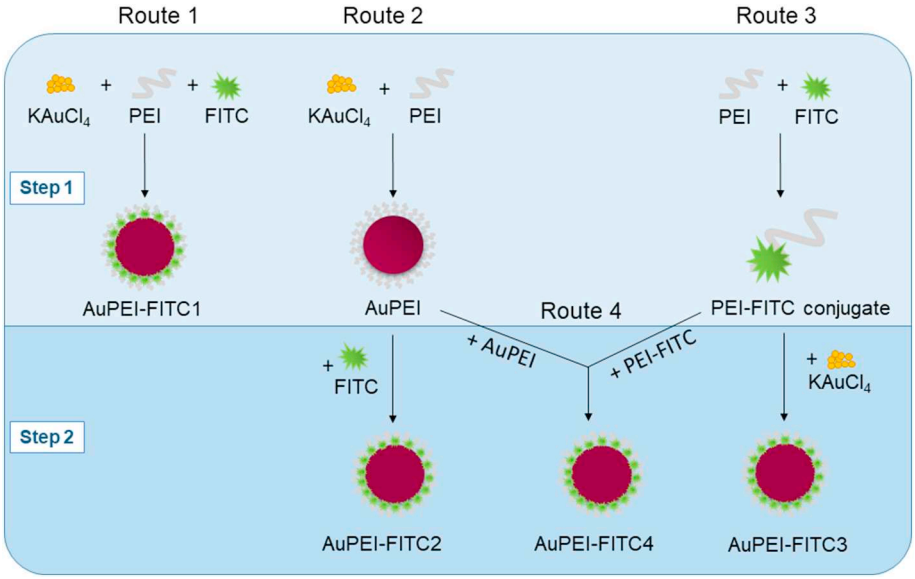

Fig. 4. Synthesis routes of AuPEI-FITC NPs.

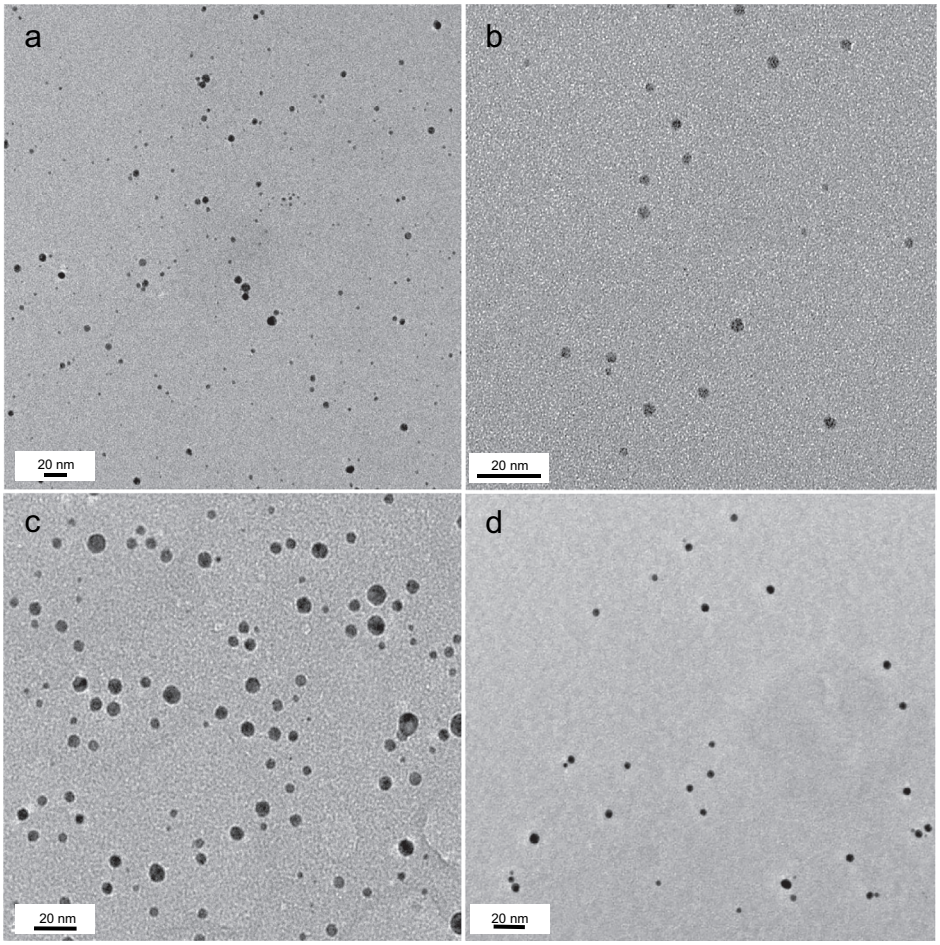

Fig. 5. TEM images of a: AuPEI-FITC1, b: AuPEI-FITC2, c: AuPEI-FITC3 and d: AuPEI-FITC4.

(Fig. S11b), showing no apparent fluorescence in the supernatants.

2.2. Cytotoxicity of AuPEI-FITC NPs

AuPEI-FITC NPs were incubated with the GBM cell lines GBM1, JHH520 and 407 at increasing concentrations for 1, 6, 12 and 24 h respectively (Fig. 7). Viability assays using the tetrazolium dye 3-(4,5-dimethylthiazol-2-yl)-2,5-diphenyltetrazolium bromide (MTT) showed that all AuPEI-FITC NPs have low impact on cell viability when added in concentrations between 0.25 and 2 mg/L, compared to untreated control cells. If NP treatment was extended for longer than 24 h, cytotoxicity of all four types of AuPEI-FITC NPs rose slightly. A possible reason for this effect can be an increased NP size or gradual loss of stabilization of the nanomaterials in culture media. Thus, we tested the stability of AuPEI-FITC NPs incubated in Dulbecco's Modified Eagle Medium (DMEM). Fig. S13 shows a rise in NP size from 118 nm to 199 nm after 3 h until a stable size of approximately 243 nm is reached between 24 and 48 h and maintained for up to two weeks of incubation in DMEM, as seen before for citrate-capped Au-NPs [31]. The greater NP size is a result of the formation of a protein corona on the surface of the NPs as they come in contact with the different proteins contained in cell culture media [32]. However, we can guarantee a stable size of the AuPEI-FITC1 system for a prolonged biomedical application. This is an important finding given that the protein corona can significantly hinder

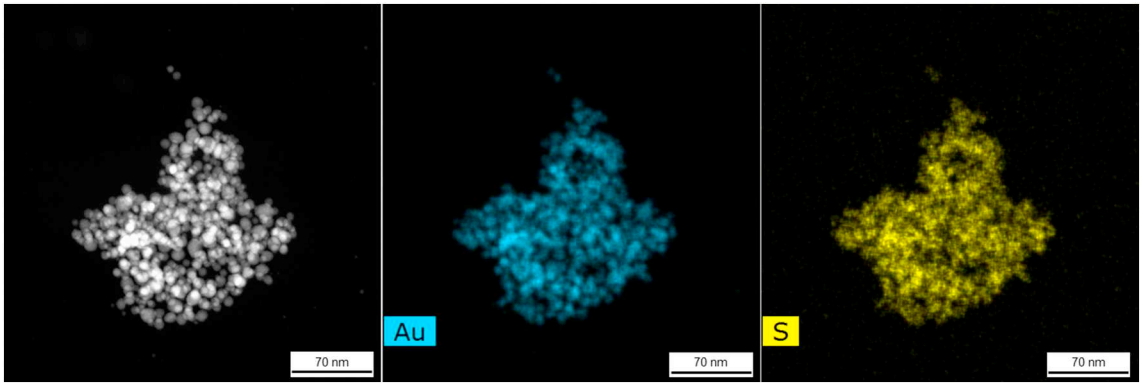

Fig. 6. STEM-EDX elemental maps of AuPEI-FITC3 showing gold (in blue) and sulfur (in yellow) atoms within the agglomerate of NPs.

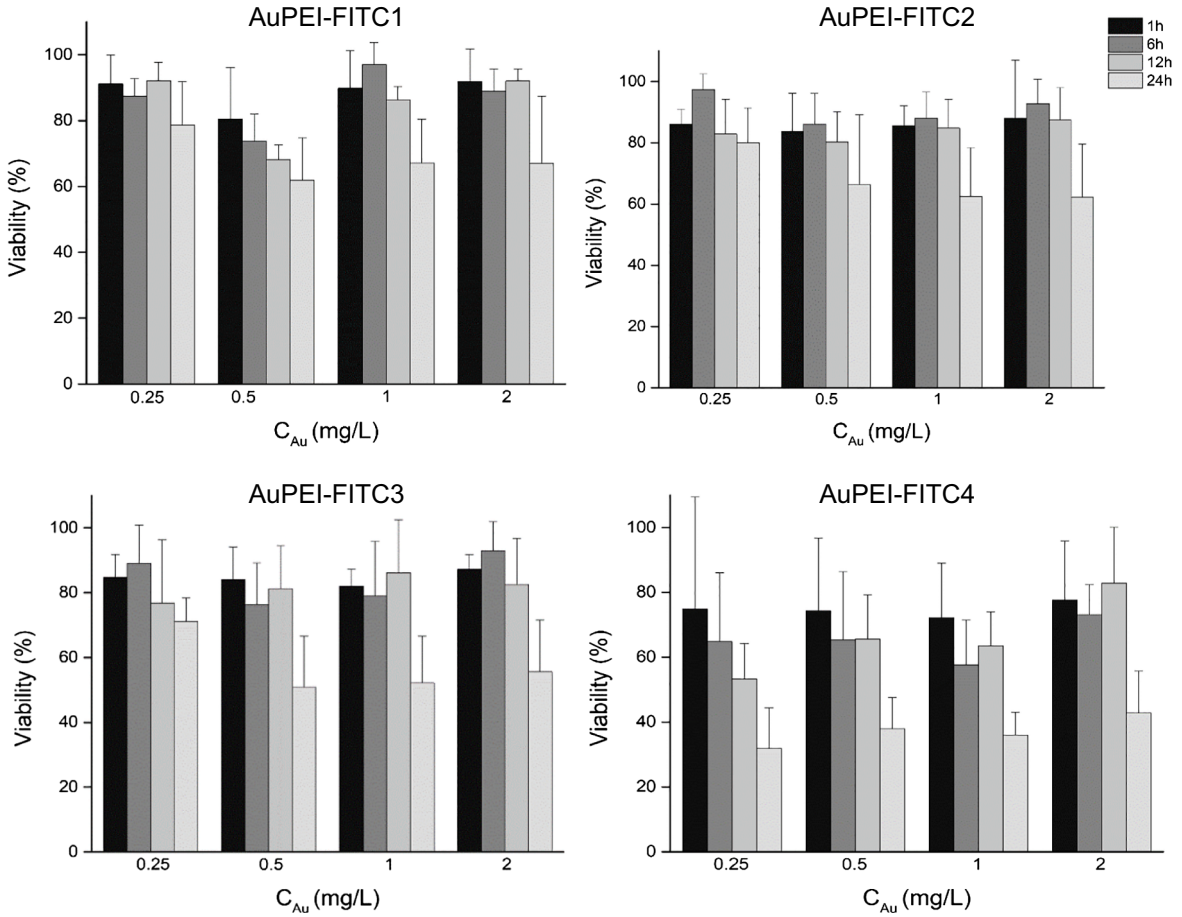

Fig. 7. Viability after 1, 6, 12 and 24 h incubation of GBM1, JHH520 and 407 cells with AuPEI-FITC NPs at increasing concentrations.

the internalization of NPs.

Other factors, such as changes in pH and ionic interactions during NP uptake processes ending in particle agglomeration and loss of their unique properties [33], could be also the reason for a lower cell viability after 24 h. Moreover, a polymer degradation and release of the PEI capping ligand from the NP surface inside the cell [34] would also account for an increased toxicity.

Additionally, our viability studies indicated some variations when incubating the same AuPEI-FITC NP sample in the different GBM cell lines. Thus, there is a dependence of the biocompatibility of AuPEI-FITC NPs on the cell type in which they were incubated. In consequence, the results displayed in Fig. 7 are sometimes widely spread around the mean value. When a mean of all concentrations and all incubation times in all cell lines was calculated (Fig. S14), AuPEI-FITC4 was identified as the least suitable for treatment with a maximum viability of only 61%. AuPEI-FITC3 showed a cell viability of 77%, whereas AuPEI-FITC1 and AuPEI-FITC2 showed values above 82%.

2.3. Uptake in glioblastoma stem-like cells

To investigate a possible uptake of AuPEI-FITC NPs into GBM stem-like cells, plated cells were investigated through a microscope after incubation, as shown in Fig. 8 for JHH520 cells treated with AuPEI-FITC4 NPs. The images in fluorescence correspond to the same area observed through a white light microscope (Fig. 8a). In these experiments, almost all neurospheres displayed fluorescent signals (Fig. 8b). This fluorescence is a result of the stable attachment of the FITC dye to the AuPEI NPs even after cell internalization. The stable dye attachment was verified through a spectroscopic investigation of the formerly internalized AuPEI-FITC1 NPs upon forced release from cells through induced osmolysis (see Fig. S15 in SI).

To rule out cell autofluorescence and to differentiate between internalized and surface-bound (adsorbed) NPs, Trypan blue quenching [35,36] was applied to inhibit extracellular fluorescence (Fig. 8c). We observed a reduction of fluorescence intensity, yet some signals remained visible after the procedure. To quantify the internalization of the NPs, we used the quantitative signal detection technology of fluorescence-activated cell sorting (FACS). In the following the term “adsorbed” refers to AuPEI-FITC NPs adhering to outside of the cell membrane (surface-bound).

2.4. Internalization of AuPEI-FITC NPs

For quantification experiments, GBM cells were treated with AuPEI-FITC NPs and measured in a buffered solution. Fig. S16 displays exemplary FACS results of untreated GBM1 cells (a), cells after incubation with AuPEI-FITC NPs (b, c) and after addition of the extracellular fluorescence quencher Trypan blue (d, e). Untreated cells showed a side scatter (SSC) under $40 \cdot 10^3$ and values lower than 10^3 when results were separated based on their fluorescence intensity (FITC scale), which can be attributed to the autofluorescence of the cells. When treated with AuPEI-FITC NPs, a new cell population (B) appeared higher on the SSC scale because of the increased complexity of cells when exposed to NPs. This population corresponded to cells which have either adsorbed only or adsorbed and internalized fluorescent NPs. As expected, such population presented higher fluorescence values due to the incorporation of the FITC fluorophore into the system. After quenching with Trypan blue, population B decreased to reveal the actual percentage of cells which have internalized fluorescent AuPEI-FITC NPs; omitting the cells with extracellular NPs (Fig. S16d, e).

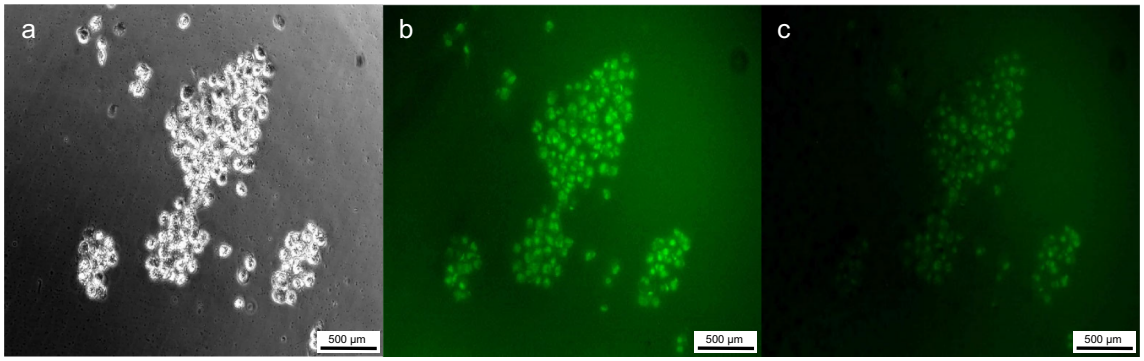

Fig. 8. Microscopic Images of JHH520 cell culture incubated with AuPEI-FITC4 NPs. Image b and c were taken using a fluorescent filter. Image b depicts the cells with adsorbed and internalized AuPEI-FITC4 NPs. Image c was taken after extracellular fluorescence quenching with Trypan blue, hence, depicts the residual internalized AuPEI-FITC4 NPs.

Moreover, analogous FSC intensities were found in both treated and untreated cells. This demonstrates again the low toxicity of our samples given that such intensity is highly dependent on cell death processes such as apoptosis.

In agreement with MTT results, FACS tests also indicated that not all cell lines react in the same way to a treatment with AuPEI-FITC NPs (Table 1). While up to 77% of JHH520 cells showed FITC fluorescence before quenching, GBM1 cells reached an adsorption plus internalization maximum of only 65% (with AuPEI-FITC4) and 407 cells yielded only 60% (with AuPEI-FITC3). From all cell lines, JHH520 cells lost the most percentage of fluorescence after quenching of the (extracellular) adsorbed AuPEI-FITC1–4 NPs. This observation highlights the importance of distinguishing between internalized and extracellular NP species. More importantly, the NP type played an even bigger role concerning their uptake in GBM cells (results after quenching). An average of the adsorbed plus internalized *versus* internalized only AuPEI-FITC NPs in all four cell lines is given at the end of Table 1. The most interesting observation was the lowest decrease in fluorescence intensity before and after quenching of AuPEI-FITC1, as well as its highest internalization average of 53% after only an hour, out of all AuPEI-FITC NPs types. Thus, this vehicle possesses the best cellular uptake potential at low NP concentrations and is hypothesized as a good candidate for treatment delivery studies against GBM.

Compliant with viability results, AuPEI-FITC4 appeared to be the most unsuitable nanocarrier, given that only ~10% of the NPs could be internalized. This realization led us to examine the nature of AuPEI-FITC4 NPs more closely. HR-TEM images revealed a polymer accumulation around the Au-NPs, sometimes even joining several gold spheres into one large agglomerate (Fig. S17). The increased amount of PEI on the NP surface would also explain the low attachment of FITC onto the AuPEI NPs and hence its lesser fluorescence intensity (Fig. S11). AuPEI-FITC4 NPs were easily adsorbed through the higher quantities of PEI polymer of AuPEI6 and the addition of the PEI-FITC conjugate (Fig. 4). This construct most likely causes strong electrostatic interactions with the cell membrane, which is negatively charged. AuPEI-FITC4 also presented the largest diameter and core size out of all AuPEI-FITC samples which probably hampers the internalization (Table S2). Overall, AuPEI-FITC4 NPs were incompatible with GBM cells, starting from their synthesis method, as they failed to well integrate the fluorescent FITC tracking system into our AuPEI NPs, contrary to the samples AuPEI-FITC1–3.

3. Conclusions

Four types of fluorescent Au-NPs with a PEI shell were reproducibly synthesized in a straight-forward manner using accessible starting materials. Gold cores sizes varied between 3 and 6 nm, according to the synthesis route. The novel one-pot method for obtaining fluorescent AuPEI-FITC NPs proved to be not only rapid and simple but also the most suitable gene vector for GBM stem-like cells. Experiments showed the importance of the synthesis method on the final morphology and internalization of gold nanocarriers. The one-pot synthesis where $KAuCl_4$, PEI and FITC were reacted together proved to be superior to two-step syntheses where two out of the three reactants were pre-reacted before being combined with the third reagents. Even though the difficulty of internalization into GBM cells remains, more than the half of the cells got nanofected for each tested cell line. Thus, we presented a quick and simple-to-adjust tool for the development of molecular-targeting Au-NPs with high clinical translational properties. Given the high chemotherapy resistance of BCSC [37], our results are promising for further experiments to develop effective drug delivery devices to eradicate that highly malignant cell population. Moreover, molecular sub-classification of brain cancers revolutionizes current neuropathology [38]. Subtype specific susceptibilities of GBM to our nanotechnology may enhance the efficacy in certain tumors. Further studies are needed to investigate any association of delivery resistance and molecular subtype. In the future, we aim to contribute to improve treatment for GBM by developing drug-conjugated vehicles equipped with epitope-specific anchor proteins such as CD133 or CD44. Efforts to attach novel discovered anti-BCSC drugs to AuPEI-NPs are underway.

Table 1
Fraction of cells with adsorbed and internalized *vs.* internalized AuPEI-FITC NPs in different GBM cell lines.[a]

Cell line	AuPEI-FITC1		AuPEI-FITC2		AuPEI-FITC3		AuPEI-FITC4	
	Adsorbed + internalized (%)	Internalized (%)	Adsorbed + internalized (%)	Internalized (%)	Adsorbed + internalized (%)	Internalized (%)	Adsorbed + internalized (%)	Internalized (%)
GBM1	63	61	56	29	52	7	65	9
JHH520	60	51	75	44	77	39	76	7
407	49	47	53	33	60	9	54	5
Average (all)	57	53	61	35	63	18	65	7

[a] 500,000 cells were incubated with 1 mg/L AuPEI-FITC NPs in PBS for 1 h. The column "Adsorbed + internalized" refers to cells before quenching. The column "Internalized" gives the fraction of cells after addition of Trypan blue solution that is quenching the extracellular NPs.

4. Experimental

4.1. Materials and methods

Branched polyethylene imine (PEI) with an average molar mass of $M_W \sim 25{,}000$ g/mol, potassium tetrachloridoaurate (III) and fluorescein isothiocyanate (FITC) were purchased from Sigma Aldrich and used without further purification. Water for the reactions was purified using the Milli-Q® purification system. Dialysis was performed using Spectra/Por® membranes from Spectrum Laboratories with a MWCO of 3.5 kDa and 50 kDa. To increase the water solubility of FITC, 50 mg (0.13 mmol) were solved in dimethyl sulfoxide (DMSO) (Honeywell, 99.7% purity) to create a FITC solution with a concentration of 4 mg/mL. This solution was then diluted to 0.05 mg/mL either in water (*FITC stock 1*) or PBS (Gibco, #10010015, Thermo Fisher Scientific, USA) buffer (*FITC stock 2*) before adding it to the nanoparticle synthesis reaction.

4.2. NP characterization

4.2.1. Transmission electron microscopy (TEM)

Sample preparation consisted on dropping 10 μL of the gold solution onto a 200 μm carbon-coated copper grid and allowing it to dry in air. TEM images were acquired on a FEI Tecnai G2 F20 electron microscope operated at 200 kV accelerating voltage and recorded with a Gatan UltraScan 1000P camera. This microscope was also used to record selected area electron diffraction (SAED) patterns. An area with sufficient material was put inside the round aperture and illuminated with widespread parallel beam to obtain focused diffraction patterns. Images were calibrated using Debye-Scherrer patterns recorded from a gold reference sample (S106, Plano GmbH, Wetzlar, Germany). High resolution TEM of gold NPs was performed using a Titan Themis 60-300 X-FEG microscope equipped with an image corrector and operated at 300 kV. Using the Gatan Digital Micrograph software, over 100 particles were counted to determine NP size and size distribution.

4.2.2. Scanning transmission electron microscopy (STEM)

STEM studies using a high-angle annular dark-field (HAADF) detector from 73 mrad to 350 mrad in combination with energy-dispersive X-ray (EDX) mapping were carried out in the Titan Themis 60–300 X-FEG microscope with a ~150 pA current, a convergence semi-angle of ~23.8 mrad and a beam size of ~0.1 nm.

4.2.3. Dynamic light scattering (DLS)

The hydrodynamic diameters of Au-NPs were determined using a Zetasizer instrument (Malvern Nano S Zetasizer) with a HeNe laser at a wavelength of 633 nm. Three measurements with four runs were assessed to calculate the mean size value.

4.2.4. Ultraviolet–visible spectroscopy (UV–VIS)

Gold nanoparticle samples were measured as synthesized on a UV-2450 spectrometer and analyzed using the UVProbe software, both from Shimadzu.

4.2.5. Fluorescence spectroscopy

300 μL of gold solution were diluted in 3 mL PBS, placed in quartz glass cuvettes and measured on a FluoroMax-4 Spectrofluorometer from HORIBA Scientific with an excitation of 490 nm.

4.2.6. Thermogravimetric analysis (TGA)

FITC decomposition studies were carried out on a Netzsch TG209 F3 Tarsus (Netzsch, Selb, Germany) instrument under a nitrogen atmosphere with a ramp between 1 and 1000 °C.

4.3. Synthesis of PEI-coated gold nanoparticles (AuPEI)

50 mg (2 μmol) of PEI were dissolved in 50 mL water and added to a round bottom flask containing a specific amount of the gold precursor $KAuCl_4$ corresponding to a n_{KAuCl4}/n_{PEI} molar ratio between 1 and 10. The yellow solution was placed in a microwave (CEM, Discover) equipped with a reflux unit and irradiated for 2 min at 100 °C and 300 W while stirring. Dialysis of the red solution was done against water for 24 h using a 50 kDa tube.

4.4. Synthesis of fluorescent gold nanoparticles (AuPEI-FITC)

4.4.1. AuPEI-FITC1

4.5 mg (12 μmol) of $KAuCl_4$ and 5 mL of *FITC stock 1* were added to a solution of 50 mg (2 μmol) of PEI dissolved in 50 mL of water and irradiated in the microwave for 2 min at 100 °C. Dialysis through a 50 kDa membrane against water for 24 h was performed as a purification step.

4.4.2. AuPEI-FITC2

4.5 mg (12 μmol) of $KAuCl_4$ were added to a solution of 50 mg (2 μmol) of PEI dissolved in 50 mL of water, irradiated in the microwave for 2 min at 100 °C and dialyzed through a 50 kDa membrane against water for 24 h. 5 mL of *FITC stock 1* were added to the AuPEI NP solution, stirred at room temperature for 8 h and dialyzed through a 3.5 kDa membrane against PBS for 24 h.

4.4.3. AuPEI-FITC3

5 mL of *FITC stock 2* were added to a solution of 50 mg (2 μmol) of PEI in 50 mL of PBS. The FITC-PEI solution was stirred at room temperature for 8 h and dialyzed through a 3.5 kDa membrane against PBS for 24 h. Afterwards, 4.5 mg (12 μmol) of $KAuCl_4$ were added, the solution was irradiated for 2 min at 100 °C and dialyzed through 3.5 kDa membrane against PBS for 24 h.

4.4.4. AuPEI-FITC4

4.5 mg (12 μmol) of $KAuCl_4$ were added to a solution of 50 mg (2 μmol) of PEI dissolved in 50 mL of water, irradiated in the microwave for 2 min at 100 °C and dialyzed through a 50 kDa membrane against water for 24 h. Volume was adjusted to 40 mL. 5 mL of *FITC stock 2* were added to a solution containing 50 mg (12 μmol) of PEI in 10 mL of PBS, stirred at room temperature for 8 h and dialyzed through a 3.5 kDa membrane against PBS for 24 h. AuPEI NP and FITC-PEI solutions were combined, stirred at room temperature for 8 h and dialyzed through a 3.5 kDa membrane against PBS for 24 h.

For synthesis details about samples AuPEI-FITC5–10, refer to Table S1 in Supp. info.

4.5. Cell cultures

Human embryonic kidney (HEK) cells are cultured in Dulbecco's Modified Eagle Medium (DMEM) without pyruvate (Gibco, #11965092, Thermo Fisher Scientific, USA) supplemented with 10% fetal calf serum (Gibco, #26140079, Thermo Fisher Scientific, USA). Glioma (BCSC) cells JHH520 cells were generously provided by G. Riggins (Baltimore, USA), GBM1 by A. Vescovi (Milan, Italy) and 407 by M.S. Carro (Freiburg, Germany). BCSC neurospheres were cultured in DMEM without pyruvate (Gibco, #11965092, Thermo Fisher Scientific, USA), 30% Ham's F12 Nutrient Mix (Gibco, #11765047), 2% B27 supplement (Gibco, #17504044), 20 ng/mL human basic fibroblast growth factor (Peprotech, #AF-100-18B, USA), 20 ng/mL human epidermal growth factor (Peprotech, #AF-100-15), 5 μg/mL Heparin (Sigma, #H0878, Merck KGaA, Germany). Both media contained 1× Antibiotic-Antimycotic (Gibco, #15240096). Cells are tested for their absence of mycoplasma contamination and validated for their genetic identity using short tandem repeat analysis similar as described before

using the core facility service of our institute [21].

4.6. Cell viability assay

96-well plates were coated with a laminin-PBS solution (1:20 v:v) (Sigma-Aldrich, # 2020, Germany) and left to dry in the sterile working bench. Each well was loaded with 20,000 GBM cells suspended in 100 µL culture medium. After successful cell adhesion on the bottom, medium was removed from each well and cells were incubated for 1, 6, 12 and 24 h with a nanoparticle:medium dilution at different concentrations. The gold concentration of the nanoparticle solutions was estimated assuming that all 12 µmol of $KAuCl_4$ were completely reduced to Au^0. A solution of 5 mg/mL MTT in PBS was diluted 1:10 in medium and added to each well (100 µL) after removal of the nanoparticle dilutions and washing each well with PBS. Allowing 90 min reaction time, MTT was taken out and 50 µL DMSO were pipetted to release the purple color. Absorbance was measured at 550 nm on an iMark™ Microplate Reader using the Microplate Manager® software from Biorad.

4.7. Nanoparticle uptake by GBM cells

500,000 glioblastoma cells were suspended in 500 µL PBS and incubated with nanoparticle dilutions at 1 mg/L for 1 h. To quench extracellular fluorescence, a 0.4% Trypan Blue solution (Sigma-Aldrich, # T8154, Germany) was added to the cell suspension in a 1:3 volume ratio. FACS measurements were performed on a BD FACSCanto™ flow cytometer equipped with blue (488 nm, air-cooled, 20 mW solid state) and red (633 nm, 17 mW HeNe) excitation sources and the FACSDiva™ software. Kaluza Analysis Software from Beckman Coulter was used for further analysis of scattering plots.

Declaration of competing interest

The authors declare that they have no known competing financial interests or personal relationships that could have appeared to influence the work reported in this paper.

Acknowledgments

The authors thank N. Stoecklein, Department of Surgery, Universitätsklinikum Düsseldorf (UKD) and his team for the technical support and providing the FACS infrastructure. We acknowledge Dr. Juri Barthel at the Ernst Ruska-Centre, Forschungszentrum Jülich GmbH (FZ Jülich), Germany for his technical support at the TEM facility under project number ER-C A-060. We thank Dr. Dirk Bier from FZ Jülich and Dr. Evmorfia Petropoulou from UKD for their helpful knowledge and help in this project. U.D. Kahlert thanks H.J. Steiger for his continuous support.

Appendix A. Supplementary data

The Supporting Information contains IR spectra, size and size distributions for NPs, details on synthesis and purification, viability plots, UV-Vis spectra, STEM-EDX for AuPEI-FITC NPs, stability characterizations, determinations of ratio of fluorescent NPs and of amounts of AuNPs in cells. Supplementary data to this article can be found online at https://doi.org/10.1016/j.jinorgbio.2019.110952.

References

[1] U.D. Kahlert, S.M. Mooney, M. Natsumeda, H.-J. Steiger, J. Maciaczyk, Int. J. Cancer 140 (2017) 10–22.
[2] Y. Yang, I.-Y. Hsieh, X. Huang, J. Li, W. Zhao, Front. Pharmacol. 7 (2016) 477.
[3] J.D. Lathia, S.C. Mack, E.E. Mulkearns-Hubert, C.L.L. Valentim, J.N. Rich, Genes Dev. 29 (2015) 1203–1217.
[4] B.G. Harder, M.R. Blomquist, J. Wang, A.J. Kim, G.F. Woodworth, J.A. Winkles, J.C. Loftus, N.L. Tran, Front. Oncol. 8 (2018) 462.
[5] S.S. Kim, A. Rait, F. Rubab, A.K. Rao, M.C. Kiritsy, K.F. Pirollo, S. Wang, L.M. Weiner, E.H. Chang, Mol. Ther. 22 (2014) 278–291.
[6] A. Orza, O. Soriţău, C. Tomuleasa, L. Olenic, A. Florea, O. Pana, I. Bratu, E. Pall, S. Florian, D. Casciano, A. Biris, Int. J. Nanomedicine 8 (2013) 689–702.
[7] I. Naletova, L.M. Cucci, F. D'Angeli, C.D. Anfuso, A.M. Magrì, D. La Mendola, G. Lupo, C. Satriano, Cancers 11 (2019) 1322, , https://doi.org/10.3390/cancers11091322.
[8] T.-M. Sun, Y.-C. Wang, F. Wang, J.-Z. Du, C.-Q. Mao, C.-Y. Sun, R.-Z. Tang, Y. Liu, J. Zhu, Y.-H. Zhu, X.-Z. Yang, J. Wang, Biomaterials 35 (2014) 836–845.
[9] Y. Zhong, C. Wang, R. Cheng, L. Cheng, F. Meng, Z. Liu, Z. Zhong, J. Control. Release 95 (2014) 63–71.
[10] G. Yang, S. Xiang, K. Zhang, D. Gao, C. Zheng, F. Zhao, Int. J. Clin. Exp. Med. 9 (2016) 753–759.
[11] D.Y. Joh, L. Sun, M. Stangl, A.A. Zaki, S. Murty, P.P. Santoiemma, J.J. Davis, B.C. Baumann, M. Alonso-Basanta, D. Bhang, G.D. Kao, A. Tsourkas, J.F. Dorsey, PLoS One 8 (2013) e62425, , https://doi.org/10.1371/journal.pone.0062.
[12] L. Bobyk, M. Edouard, P. Deman, M. Vautrin, K. Pernet-Gallay, J. Delarochea, J.-F. Adam, F. Estève, J.-L. Ravanat, H. Elleaume, Nanomed.-Nanotechnol. 9 (2013) 1089–1097.
[13] M.F. Kircher, A. de la Zerda, J.V. Jokerst, C.L. Zavaleta, P.J. Kempen, E. Mittra, K. Pitter, R. Huang, C. Campos, F. Habte, R. Sinclair, C.W. Brennan, I.K. Mellinghoff, E.C. Holland, S.S. Gambhir, Nat. Med. 18 (2012) 829–834.
[14] W. Shang, C. Zeng, Y. Du, H. Hui, X. Liang, C. Chi, K. Wang, Z. Wang, J. Tian, Adv. Mater. 29 (2017) 1604381.
[15] X. Gao, Q. Yue, Z. Liu, M. Ke, X. Zhou, S. Li, J. Zhang, R. Zhang, L. Chen, Y. Mao, C. Li, Adv. Mater. 29 (2017) 1603917.
[16] L. Zhao, S. Wen, M. Zhu, D. Li, Y. Xing, M. Shen, X. Shi, J. Zhao, Artif. Cell Nanomed. B. 46 (2018) 488–498.
[17] I. Fratoddi, I. Venditti, C. Cametti, M.V. Russo, J. Mater. Chem. B 2 (2014) 4204–4220.
[18] M. Saito, H. Saitoh, Biosci. Biotechnol. Biochem. 76 (2012) 1777–1780.
[19] X. Sun, S. Dong, E. Wang, J. Colloid Interface Sci. 288 (2005) 301–303.
[20] S.-C. Wei, P.-H. Hsu, Y.-F. Lee, Y.-W. Lin, C.-C. Huang, ACS Appl. Mater. Interfaces 4 (2012) 2652–2658.
[21] U.D. Kahlert, A.K. Suwala, E.H. Raabe, F.A. Siebzehnrubl, M.J. Suarez, B.A. Orr, E.E. Bar, J. Maciaczyk, C.G. Eberhart, Brain Pathol. 25 (2015) 724–732.
[22] B. Devika Chithrani, A. Ghazani, W. Chan, Nano Lett. 6 (2006) 662–668.
[23] T.D. Fernández, J.R. Pearson, M.P. Leal, M.J. Torres, M. Blanca, C. Mayorga, X. Le Guével, Biomaterials 43 (2015) 1–12.
[24] E.C. Cho, L. Au, Q. Zhang, Y. Xia, small 6 (2010) 517–522.
[25] E. Panzarini, S. Mariano, E. Carata, F. Mura, M. Rossi, L. Dini, Int. J. Mol. Sci. 19 (2018) 1305–1325.
[26] W.J. Song, J.Z. Du, T.M. Sun, P.Z. Zhang, J. Wang, small 6 (2010) 239–246.
[27] M. Ortega-Muñoz, M. Giron-Gonzalez, R. Salto-Gonzalez, A. Jodar-Reyes, S. De Jesus, F. Lopez-Jaramillo, F. Hernandez-Mateo, F. Santoyo-Gonzalez, Chem. Asian J. 11 (2016) 3365–3375.
[28] M. Thomas, A.M. Klibanov, PNAS 100 (2003) 9138–9143.
[29] H.S. Choi, W. Liu, P. Misra, E. Tanaka, J.P. Zimmer, B.I. Ipe, M.G. Bawendi, J.V. Frangioni, Nat. Biotechnol. 25 (2007) 1165.
[30] S. Wang, X. Wang, Z. Zhang, L. Chen, Colloids Surf. A Physicochem. Eng. Asp. 468 (2015) 333–338.
[31] G. Maiorano, S. Sabella, B. Sorce, V. Brunetti, M.A. Malvindi, R. Cingolani, P.P. Pompa, ACS Nano 4 (2010) 7481–7491.
[32] X. Cheng, X. Tian, A. Wu, J. Li, J. Tian, Y. Chong, Z. Chai, Y. Zhao, C. Chen, C. Ge, ACS Appl. Mater. Interfaces 7 (2015) 20568–20575.
[33] B. Halamoda-Kenzaoui, M. Ceridono, P. Urbán, A. Bogni, J. Ponti, S. Gioria, A. Kinsner-Ovaskainen, J. Nanobiotechnol. 15 (2017) 48.
[34] S. Honary, F. Zahir, Trop. J. Pharm. Res. 12 (2013) 255–264.
[35] J. Hed, G. Hallden, S.G. Johansson, P. Larsson, J. Immunol. Methods 101 (1987) 119–125.
[36] S. Vranic, N. Boggetto, V. Contremoulins, S. Mornet, N. Reinhardt, F. Marano, A. Baeza-Squiban, S. Boland, Part. Fibre Toxicol. 10 (2013) 2, https://doi.org/10.1186/1743-8977-10-2.
[37] A. Eramo, L. Ricci-Vitiani, A. Zeuner, R. Pallini, F. Lotti, G. Sette, E. Pilozzi, L.M. Larocca, C. Peschle, R. De Maria, Cell Death Differ. 13 (2006) 1238–1241.
[38] D. Capper, D.T.W. Jones, M. Sill, V. Hovestadt, D. Schrimpf, D. Sturm, et al., Nature 555 (2018) 469–474, https://doi.org/10.1038/nature26000.